THE ^{4}He TRIMER: STRUCTURE AND ENERGETICS OF A VERY UNUSUAL MOLECULE

Cono Di Paola[a1], Franco A. Gianturco[a2,*], Gerardo Delgado-Barrio[b1], Salvador Miret-Artés[b2] and Pablo Villarreal[b3]

[a] *Department of Chemistry, The University of Rome, Cittá Universitaria, 00185 Rome, Italy; e-mail: [1] dipaola@caspur.it, [2] fa.gianturco@caspur.it*

[b] *Instituto de Mátematicas y Fisica Fundamental, Consejo Superior de Investigaciones Cientificas, Serrano 123, 28006 Madrid, Spain; e-mail: [1] gerardo@fam77.imaff.csic.es, [2] salvador@fam10.imaff.csic.es, [3] p.villarreal@imaff.cfmac.csic.es*

Received April 18, 2002
Accepted June 26, 2002

This work is affectionately dedicated to Petr Čársky, Ivan Hubač and Miroslav Urban, on the occasion of their 60th birthdays, with our best wishes for many more years of splendid activity in the world of scientific research.

The $^4He_3$ weakly interacting system is analysed by constructing the full interaction as a sum of two-body (2B) potentials chosen among the most recent proposals from the literature. The spatial density distributions of the three bound atoms are obtained using a diffusion Monte Carlo (DMC) algorithm and a stochastic analysis under specific geometric constraints is carried out with the resulting densities in order to recover a more conventional structural picture for such floppy system. The total binding energies were obtained with the chosen potentials analysed in the present work, using the DMC algorithm, and are compared with previous published results. The ensuing spatial distributions are analysed in some detail to select the dominant structures from a conventional triangular description of this very floppy molecule.

Keywords: Helium clusters; Two-body interaction potentials; Diffusion Monte Carlo algorithm; Stochastic analysis; Quantum chemistry; *Ab initio* calculations.

The detailed study of smaller ^{4}He clusters, in particular dimers and trimers, is an important initial step for a better understanding of the properties of helium liquid droplets, for interpreting the superfluid features in ^{4}He films and for predicting the possible occurrence of Bose–Einstein condensates involving such bosons[1–4]. The problem of evaluating the binding energies of trimers involving both ^{4}He and ^{3}He, for instance, has therefore caused renewed attention in the last few years[5–8] and has attracted a great deal of work, both experimental[9] and theoretical[10]. One of the additional interests

in the properties of the trimer clusters comes from the fact that the very small binding energy for their ground states also sparked the analysis of their excited states and of the possible existence of Efimov states[5,6,11] for such weakly bound species.

A further feature of overall properties of the ^{4}He molecular aggregates comes from the unusually large spatial delocalization of its component atoms as opposed to the more conventional shapes of Ne_3 and Ar_3 aggregates[12,13]. Thus, the discussion on the actual, most reliable value of the ground state binding energy has been coupled to the question of how to define the spatial shape of such an aggregate and how to represent it in terms of the more conventional "balls-and-sticks" description of a molecular structure (see, *e.g.*, the discussion in ref.[14]).

In the present study we decided to perform a stochastic analysis of the dominant configurations through which one could describe the spatial shape of the $^4He_3$ aggregate. In particular, we have employed some of the more recent among the many existing proposals for the two-body (2B) interatomic potentials and have used them to describe the three-particle interaction as a sum of 2B forces. The last approach has been the one most frequently adopted in the theoretical studies since it turns out to be reasonable to assume that three-body forces play a rather minor role in this system, at least for situations which are far from the bulk[8]. We have therefore carried out the calculation of the nodeless ground state wavefunction, and of various spatial observables associated with it, and have also examined the changes occurring with the different 2B potentials employed. We have computed the total binding energies by employing here the DMC algorithm discussed briefly below and compared our results with earlier findings.

THE COMPUTATIONAL METHOD

The DMC method has been extensively discussed in a number of papers[15–18]. We therefore refer the reader to that literature for a fuller discussion, while this section merely summarises the main features of the method.

The key idea consists in the isomorphism between the solutions given by a time-dependent many-body Schrödinger equation and those obtained from a multidimensional reaction-diffusion equation with anisotropic diffusion coefficients. Introducing the imaginary time $\tau = it/\hbar$, shifting the absolute energy scale by a quantity E_{ref} and identifying the inverse mass terms

with diffusion coefficients D_j and the shifted potential $[V(\boldsymbol{r}) - E_{\mathrm{ref}}]$ with a position-dependent rate term $k(\boldsymbol{r})$ lead to the following equations

$$i\hbar \frac{\partial \Psi(\boldsymbol{r},t)}{\partial t} = -\sum_j \frac{\hbar^2}{2m_j} \nabla_j^2 \Psi(\boldsymbol{r},t) + [V(\boldsymbol{r}) - E_{\mathrm{ref}}]\Psi(\boldsymbol{r},t) \qquad (1)$$

$$\frac{\partial \Psi(\boldsymbol{r},\tau)}{\partial \tau} = -\sum_j \frac{\hbar^2}{2m_j} \nabla_j^2 \Psi(\boldsymbol{r},\tau) + [V(\boldsymbol{r}) - E_{\mathrm{ref}}]\Psi(\boldsymbol{r},\tau) , \qquad (2)$$

where the last equation could be viewed as a diffusion equation plus a rate term

$$\frac{\partial C(\boldsymbol{r},t)}{\partial t} = \sum_j D_j \nabla_j^2 C(\boldsymbol{r},t) + k(\boldsymbol{r}) C(\boldsymbol{r},t) . \qquad (3)$$

Knowledge of the structure of the wavefunction can be fruitfully exploited to gain increased accuracy by introducing a guiding trial function Ψ_{T}, that is meant to approximate the true wavefunction. A common ansatz for atomic clusters and bulk systems expresses Ψ_{T} as a product over a set of one-dimensional functions Φ defined over all pairs of particles

$$\Psi_{\mathrm{T}}(\boldsymbol{r}, \boldsymbol{p}) = \prod_{i<j} \Phi_{ij}(\boldsymbol{r}_{ij}; \boldsymbol{p}) , \qquad (4)$$

where $\boldsymbol{r}_{ij}$ is the distance between particles *i* and *j*, and $\boldsymbol{p}$ denotes the set of adjustable parameters controlling the trial wavefunction. Previous experience with helium clusters[8,19] showed that Jastrow functions are a good choice for the Φ's and thus they have been employed by us in the present work. In particular, we used the same trial function already used in the earlier calculations[8].

The introduction of Ψ_{T} results in additional drift terms in the diffusion equation which direct the random walkers into regions where the trial wavefunction is large. At the same time, the rate terms are controlled by the local energy values that are given by

$$E_{\mathrm{local}}(\boldsymbol{r}) = \Psi_{\mathrm{T}}^{-1}(\boldsymbol{r}) \hat{H} \Psi_{\mathrm{T}}(\boldsymbol{r}) = \Psi_{\mathrm{T}}^{-1}(\boldsymbol{r}) \hat{T} \Psi_{\mathrm{T}}(\boldsymbol{r}) + V(\boldsymbol{r}) , \qquad (5)$$

which is a smoother function of the coordinates than the potential and reduces the variance of the energy estimators

$$\frac{\partial(\Psi\Psi_T)}{\partial\tau} = \left[\sum_j \frac{1}{2m_j}\nabla_j^2(\Psi\Psi_T) - \frac{1}{m_j}\nabla_j(\Psi\Psi_T\nabla\ln\Psi_T)\right]$$

$$-\left[\Psi_T^{-1}T\Psi_T + V(\boldsymbol{r}) - E_{\text{ref}}\right](\Psi\Psi_T)\,. \qquad (6)$$

A random walk technique is used to calculate the steady-state solution of the diffusion equation corresponding to our quantum problem. A large ensemble of random walkers (see details below) is propagated with time steps $\Delta\tau$ starting from some arbitrary initial distribution. The propagation from τ to $\tau + \Delta\tau$ consists of random Gaussian displacements of the Cartesian coordinates, of systematic moves under the influence of the quantum drift force $F(\boldsymbol{r}) = \Psi_T\nabla\ln\Psi_T$ and an update of the weight carried by each random walker. Additionally, we use a Metropolis-type acceptance check for each attempted move such that for arbitrary time steps the number density of walkers is given by Ψ_T^2 while their weights are a stochastic sample of the local value of Ψ/Ψ_T. The short time approximation to the Green's function is given by

$$G(\boldsymbol{r}\to\boldsymbol{r}';\Delta t) = \prod_j\left[\left(\frac{m_j}{2\pi\Delta\tau}\right)^{\frac{3}{2}}\exp\left\{-\frac{m_j}{2\Delta\tau}\left(\boldsymbol{r}_j - \boldsymbol{r}_j' - \frac{\Delta\tau}{2m_j}\boldsymbol{F}_j(\boldsymbol{r})\right)^2\right\}\right]$$

$$\times\exp\left\{-\Delta\tau_{\text{eff}}\left(\frac{E_{\text{local}}(\boldsymbol{r}) + E_{\text{local}}(\boldsymbol{r}')}{2} - E_{\text{ref}}\right)\right\}. \qquad (7)$$

The modified time step $\Delta\tau_{\text{eff}}$ appears in the growth term of Eq. (*5*) because not all moves attempted according to $G(\boldsymbol{r}\to\boldsymbol{r}';\Delta\tau)$ are accepted in the Metropolis step[17]. Proposed moves from $\boldsymbol{r}$ to $\boldsymbol{r}'$ are then carried out with probability

$$P(\boldsymbol{r}\to\boldsymbol{r}') = \min\{1, A(\boldsymbol{r}\to\boldsymbol{r}')\} \qquad (8)$$

$$A(\boldsymbol{r}\to\boldsymbol{r}') = \frac{|\Psi_T(\boldsymbol{r}')|^2\,G(\boldsymbol{r}'\to\boldsymbol{r})}{|\Psi_T(\boldsymbol{r})|^2\,G(\boldsymbol{r}\to\boldsymbol{r}')}\,. \qquad (9)$$

Walkers whose relative weight $w_{rel} = w_i/W(\tau)$ falls below a preselected value w_{min} are eliminated randomly from the ensemble with probability $p_- = 1 - w_{rel}$. Here $W(\tau) = \Sigma_i w_i(\tau)$ is the sum of weights[20,21]. Walkers whose relative weight fall above that value are retained and assigned the average weight $W(\tau)/n_{walk}$ with probability $p_+ = w_{rel}$. Walkers whose relative weight grows beyond a maximum value w_{max} are split into $n_w = \mathrm{int}(w_{rel} + u)$ walkers of weight w_i/n_w, where u is a uniform random number. The values of w_{min} and w_{max} are chosen such that the average number of walkers remains approximately constant during the run, while the instantaneous ensemble fluctuates. These mechanisms ensure that the walkers remain concentrated in relevant regions of configuration space without introducing artificial sources or sinks. After equilibration of the initial random walker distribution, the ensemble average of E_{local} becomes identical with the ground state energy irrespective of Ψ_T and is only subject to statistical fluctuations. The ground state energy can also be computed from the rate at which the total weight of the ensemble grows or decays as τ elapses.

In order to take into account the slow decay of the weak He–He interaction terms as the distances increased, we have employed extended temporal runs that ensure the correct sampling of the full PES by the random walkers (for details, see below).

Arbitrary property expectation values $\langle \hat{A} \rangle$ are computed by replacing integrals by sums over samples

$$\langle \hat{A} \rangle = \frac{\int \Psi^*(\boldsymbol{x}) \hat{A} \Psi(\boldsymbol{x}) \, \mathrm{d}\boldsymbol{x}}{\int |\Psi(\boldsymbol{x})|^2 \, \mathrm{d}\boldsymbol{x}} \tag{10}$$

$$\approx \frac{1}{N} \sum_{i=1}^{N} \Psi^{-1}(\boldsymbol{x}) \hat{A} \Psi(\boldsymbol{x}) \,, \tag{11}$$

where $\boldsymbol{x}$'s indicate some general coordinates and the correct $|\Psi|^2$ quantity is obtained from the estimated, trial Ψ_T values. Expectation values of local operators are directly accessible with the DMC scheme. In this case the integration reduces to an average over operator values $A(\boldsymbol{x})$

$$\langle \hat{A} \rangle \approx \frac{\sum_i^N w_i A(\boldsymbol{x}_i)}{\sum_i^N w_i} \,. \tag{12}$$

The radial distribution of rare-gas atoms relative to the center of mass of the trimer is computed as

$$P_{\mathrm{rad}}(R) = \frac{1}{n}\sum_{i}^{n} \left\langle \frac{\partial(R_i - R)}{R^2} \right\rangle_{\mathrm{walk}} . \qquad (13)$$

The radial distribution function can be easily converted to the spherically averaged radial rare-gas density distribution $\rho(R)$

$$\rho(R) = \frac{n}{4\pi} P_{\mathrm{rad}}(R) \qquad (14)$$

with n being the number of atoms in the aggregate.

One can further obtain, using the same procedure, the angular distributions associated with ϑ, corresponding to counting all the possible angles between two bonds originating from any of the three atoms, ϑ_{ij}, with the normalization condition

$$\int_{-1}^{1} P_{\mathrm{tot}}(\cos\vartheta)\,\mathrm{d}\cos\vartheta = 1 \qquad (15)$$

From the above one can also extract directly the angular dependence, subject to the same condition

$$\int_{\pi}^{\pi} P_{\mathrm{tot}}(\vartheta)\,\mathrm{d}\vartheta = 1 \qquad (16)$$

and from it the distributions for each of the three ϑ_{ij} angles of all the configurations which are found to contribute to the final wavefunction for the ground state.

In all the calculations we used an ensemble of variable size kept at an average size of 2000 random walkers by a proper choice of $w_{\min}$ and $w_{\max}$. The time step length was carefully checked for eliminating the time step bias and an optimal value of 25 a.u. was found and used in all the calculations. The effective time steps were very close to the nominal time step with $\Delta\tau_{\mathrm{eff}}$ never smaller than 0.98 $\Delta\tau$. Given an initial random distribution of walkers, the ensemble was propagated for several thousands of steps in order to equilibrate it and then the energy estimators were collected over blocks with a typical length of 8000 steps. The serial correlations between block averages were carefully analysed by calculating the autocorrelation functions in order to be sure that the final average was taken over independent

blocks. All the averages were therefore calculated using a variable number of blocks depending on the cluster size with a typical value of at least 500 blocks.

THE TWO-BODY INTERACTION POTENTIALS

As mentioned above, the last few years have witnessed a dramatic increase in the number of papers dedicated to the theoretical investigation of the molecular clusters containing ^{4}He. Most of those investigations consist of the computation of the trimer ground state energy and are based on different approaches to the problem. Thus, some are based on variational methods[6,8,19,22–24] while others employ a hyperspherical harmonics expansion in configuration space[5,13,25] or an integral equation formulation in momentum space[26,27]. Further results were also obtained with a direct solution of the two-dimensional Faddeev equations in configuration space[28] or by using the three-dimensional Faddeev differential equations in the total angular momentum representation[29]. Very recently, the binding energy of $^4He_3$ was obtained using several 2B potentials and a hard-core version of the Faddeev differential equations[10].

All the above calculations produced a variety of values for the binding energy of $^4He_3$ but, in most cases, either did not dwell on the expected shape of the aggregate or simply made some general, vaguely qualitative consideration on the configurations which were likely to dominate the cluster description. In addition, an equally broad variety of atom–atom interaction potentials were employed to carry out the calculations and therefore a detailed comparison between different results becomes even more complicated.

In the present work we decided to employ four specific interatomic potentials which have been recently suggested and which have all been tested before with at least one of the theoretical methods listed above. We started with the DMC procedure to generate ground state wavefunctions and employed them to see how such a floppy three-atom bound system could be realistically described.

The oldest of the tested potentials is the one which we label here, in accord with common usage, the Hfd-b (He) potential of Aziz and others[30]. The latter form was fitted to low-temperature second virial coefficients data and accurate viscosity data obtained at room temperature, while at the same time pinning the repulsive wall to the value computed by Ceperley and Partridge[17] at 1 a_0. Such potential reproduced, within experimental errors, viscosities and thermal conductivities, differential cross sections,

high-energy cross sections and backward glory oscillations. A further modification of the above potential was obtained by taking into consideration additional *ab initio* data and by extending the range of experimental observables which could be reproduced by the modification[32]. It will be called here the LM2M2 potential form.

More recently, a very accurate analytic representation of the He–He interaction, based on perturbation theory, has been given[33] and widely used in theoretical computations of the very last years. It will be used in the present work with the acronym of TTY.

One final choice of the 2B interaction potential comes from a different calculation based on the surface integral method[34,35] and recently applied to He-alkali atoms interactions[36]. It will be called the KTTY potential in the present work.

Just to provide a qualitative, pictorial comparison of the four potential curves which we employ in our analysis, we report in Fig. 1 the radial behaviour of such model 2B interactions. The left-hand panel in the figure

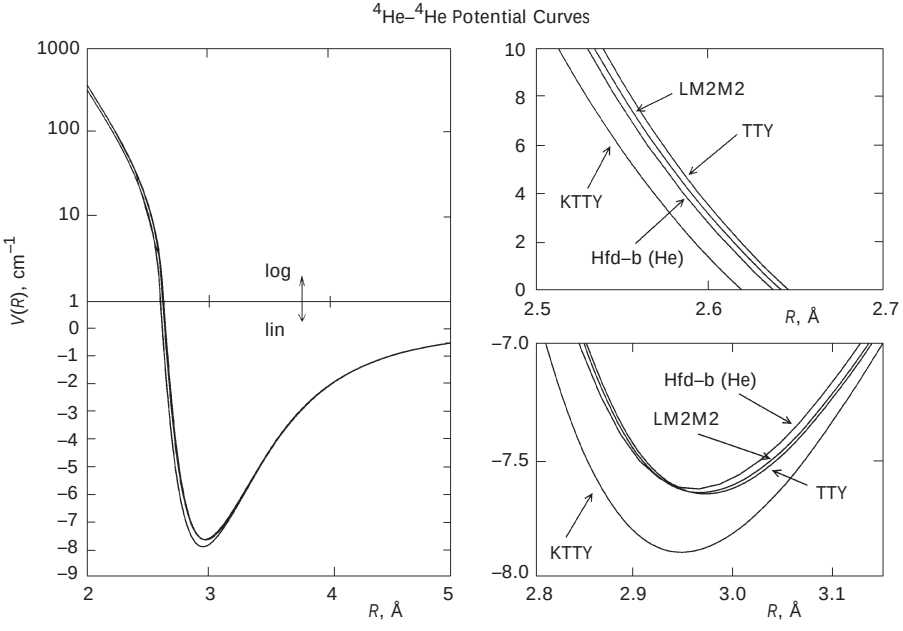

FIG. 1

Potential energy curves of the $^4He_2$ system employed in the present work. Left panel: overall shapes of the four 2B potentials. Right panels: the upper part shows the onset of the repulsive walls while the lower part reports the region of the attractive wells. The acronyms of the potentials are explained in the main text

shows the overall shapes of all four potentials, their well regions given on a linear energy scale while their repulsive parts are given on a log scale. The two panels on the right in the same figure show instead the detailed comparison between the shapes of their repulsive walls up to 10 cm^{-1} (upper panel) and the same comparison between the depths and positions of their attractive wells (lower panel). The following considerations could be easily made:

(i) three of the potential functions exhibit very similar behaviour of their low-energy repulsive walls, with the exception of the KTTY potential which clearly shows a much softer shape and smaller turning points than the others;

(ii) the well regions of the same three potentials as above are again very close to each other, with the TTY interaction being the largest and with its minimum value at the largest distance. On the other hand, the KTTY potential is markedly stronger and presents a much deeper attractive well, with its minimum position located at a smaller distance. It is interesting to notice that the latter 2B potential is very different from the latest quantum calculations which were deemed by the authors[15,37] to be essentially exact. We would also like to point out that other recent calculations[38] for the total energy of the helium dimer have produced a value in excellent agreement with the Anderson's results[37], thus leaving no doubt that the later two potentials are providing the best energy estimators for the dimer molecule. We will see below that the above differences will be reflected in the final values of the binding energies for the trimer ground states, while affecting very little the general spatial properties of the corresponding wavefunctions. This point is particularly important for the analysis which we have carried out in the present system.

We also present in Fig. 2 the behaviour of the estimated total minimum energy (D_e) for each potential curve discussed in this work and of the corresponding binding energy (E_b) obtained for the same set of potentials, as we shall discuss below. The upper panel of the figure reports the D_e values and also the zero-point-energy (ZPE) values as obtained from the E_b values of the lower panel: $D_e - D_0$ = ZPE. One clearly sees here the very large quantum effects coming from the dominance of the ZPE values over the strength of the interaction, a feature that gives already indications of the marked spatial delocalization of the three nuclei discussed in the following.

RESULTS AND DISCUSSION

The Angular Distributions

The converged calculations through the walkers propagation allow one to obtain the final distributions for several properties of the trimer which can help to analyse better the meaning of familiar concepts like “structure” or “spatial arrangement” for the three bound atoms of this unusual system. We will also extract additional microscopic properties of the DMC wavefunctions which have never been obtained before by other calculations on the present system. In Fig. 3 we report the results of the calculations for the angular distributions from one of the four 2B potentials employed here, the TTY potential: all other 2B interactions behave essentially in the same way, with only minor differences, as we will further discuss below. The two reported panels show the same type of results, *i.e.* we give on the right-hand

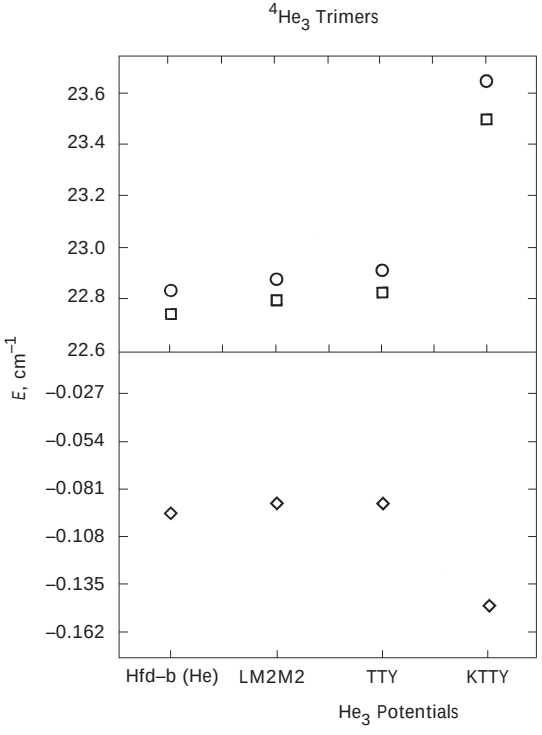

FIG. 2

Comparison of computed binding energies (E_b) from the 2B potential choices (lower panel) and of the zero-point-energy (ZPE) values with the global potential minimum, D_e, for the four potential functions (upper panel). ○ $D_e = -V_{min}$, □ ZPE; ◇ $E_b = -D_0$

panel the total distribution of the cosines of any of the angles formed in each triangular arrangement at the end of the calculations. Each distribution $P_{tot}(\cos\vartheta)$ is normalized as discussed earlier and the range of the values of the cosines is shown in each panel. Because of the fairly minor differences exhibited by the different 2B potentials, we only report in the figure the behaviour of one of them, although the calculations were carried out with all four potentials. It is interesting to make the following observations:

(i) the distribution presents a clear maximum in the region of the $\cos\vartheta$ values approaching 1.0 (≈0.96) indicating a marked dominance of configurations containing at least one angle lower than 10°, *i.e.* close to giving a quasi-collinear structures. However, the actual configurations with ϑ being 0°, which need to be matched by a corresponding set of configurations at 180° (*i.e.* for $\cos\vartheta \approx -1.0$) are present but are much less prominent;

(ii) the general behaviour of the computed distributions is the one in which the contributing weights of angular values from 180° to ≈0° steadily increase, with a very marked gradient increase beyond ≅60°.

The above properties of the $P_{tot}(\cos\vartheta)$ already indicate, albeit only tentatively, that the dominant configurations do not appear to be equilateral

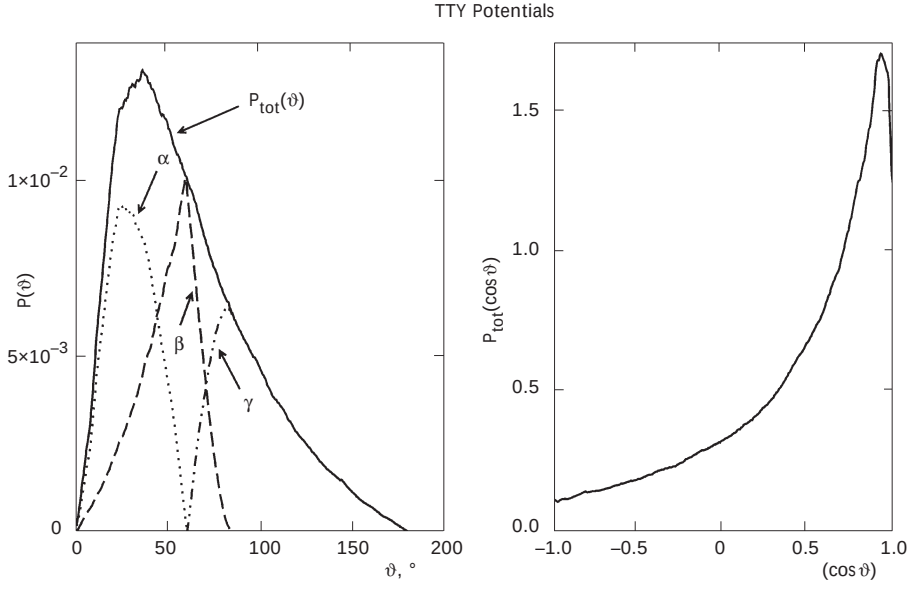

FIG. 3

Computed angular distributions from DMC calculations using the TTY 2B potential of ref.[33] Right panel: $P_{tot}(\cos\vartheta)$ distribution; left panel: angular distributions for the sum of the angles (ϑ) and for each of the angles in the triangular configurations

triangles as common sense might suggest, and as recently suggested by calculations that used the hyperspherical coordinate approach in the adiabatic approximation[13]. We further indicate that the collinear arrangements, characterized by the presence of nonvanishing probability values for $\cos\vartheta = 1.0$ and –1.0, are indeed present, as suggested by earlier DMC calculations[8,19,39], but do not appear to be the dominant configurations within the distribution. One further piece of information which we could also gather from our final results is obtained by separating, using all the configurations in the final distributions, the relative span of each of the three angles and of their sum. Such distributions are obviously related to the cosine distributions discussed earlier by a simple relationship obtained from the normalisation condition of Eq. (*16*) from which we get: $P(\vartheta) = P(\cos\vartheta)\sin\vartheta$.

The corresponding results are given, for each of the three angles and for their sums, in the left-hand panels of the same Fig. 3. The choice has been made of labelling as α the smallest of the three angles, β the intermediate value and as γ the largest. The following can be gleaned from that panel:

(i) the overall maximum of the angles from all the contributing configurations, and for all the different potentials, is around 35°. This datum appears to confirm that the equilateral configurations (with $\vartheta \approx 60°$) are not dominating in the description of this quantum trimer[13];

(ii) the region where β shows a maximum (*i.e.* around 60°) is a special region since the sequential constraint in the sampling ($\alpha < \beta < \gamma$) causes the ($\alpha = 60°$, $\gamma = 60°$) situation to be negligible, while we can still have many contributions and a strong peak for β at 60°. In other words, the equilateral configurations are probably contributing but not very much, and therefore hardly show up on the scale of our distributions;

(iii) the region of both α and β approaching 0° corresponds to a very marked drop of probability values, as also happens when γ is approaching 180°. Although such behaviour comes from the $\sin\vartheta$ factor which multiplies the $P(\cos\vartheta)$, the overall lack of marked contributions from collinear arrangements also confirms what was seen in the behaviour of $P(\cos\vartheta)$ discussed before;

(iv) the largest of the angles in each contributing configuration clearly indicates sizeable probability contributions, as expected, beyond $\vartheta \approx 90°$ and therefore suggests the presence of either isosceles or scalene structures which are not far from the collinear arrangement. This feature is probably causing the large contributions from $\alpha \leq 20°$, shown by the smallest angle, and the sizeable contributions with $\beta < 40–50°$ appearing in the panels. Such distributions, in fact, tell us that the scalene configurations where two ^{4}He atoms are closer to each other than the third atom are very important.

Table I reports several expectation values of the angular parameters in its lower part to confirm both the similar behaviour of all four potentials and the fairly large standard deviations existing for the angular variables, a further indication of the remarkable floppiness shown by the structure of this system.

The Radial Distributions

As already mentioned before, the actual location of the bound atoms in terms of various choices of relative distances can also be obtained from the DMC calculations. Thus, from the final configurations given by each of the 2B potentials, we have computed the distributions of the atom–atom distances $P(r)$ as defined in the previous Section. We also obtained the radial distribution in units of Å^{-1} by evaluating $P(r) \times r^2$. Furthermore, we can generate radial locations for the three atoms as taken from the center-of-mass (r_{cm}) of each trimer configuration and their corresponding values in Å^{-1}, $P(r_{cm}) \times r_{cm}^2$. All the above quantities were obtained for each of the potentials employed and are shown in the four panels appearing in Fig. 4 for the case of the TTY potential.

TABLE I
Expectation values of geometric parameters (Å, °) for the trimer systems studied in this work. The standard deviation values are also shown

Parameter	LM2M2	HfdB–(He)	TTY	KTTY
$\langle r^2 \rangle$	43.47	43.05	42.99	41.10
$\langle r \rangle$	5.90	5.87	5.90	5.74
$\langle r^2 \rangle^{1/2}$	6.56	6.59	6.56	6.41
$\langle \Delta r \rangle$	2.94	2.92	2.86	2.85
$\langle \alpha \rangle$	29.6	29.6	30.3	29.7
$\langle \Delta\alpha \rangle$	12.7	12.6	12.5	12.7
$\langle \beta \rangle$	48.5	48.5	49.1	48.6
$\langle \Delta\beta \rangle$	16.4	16.3	15.9	16.4
$\langle \gamma \rangle$	101.9	101.9	100.5	101.6
$\langle \Delta\gamma \rangle$	25.3	25.3	24.7	25.3
$\langle$cos HeHeHe$\rangle$	0.60	0.60	0.60	0.60

The calculations exhibit the same behaviour for all four potentials, thereby confirming that the tiny differences among them are affecting binding energy values (see Table III below) much more than other observables related to configurational weights, where the PES differences do not alter much the final wavefunctions. Our results confirm the findings about radial distributions obtained in earlier work[8,12,13], while also showing some differences that we will discuss below:

(i) the radial distributions of the atom–atom distances, in the upper-left panels, show the sudden drop of values when any of the atoms approaches the repulsive wall (at ≈3 Å) of the 2B interaction. These distributions further exhibit their maximum around 4 Å, as in earlier work[8,12,13];

(ii) the distributions weighted by r^2 (lower-left panels) appear to be much broader after normalization and extend out to ≈100 Å. This feature indeed confirms the very extended spatial distribution of the bound trimer and the very flexible nature of its structural properties: as an example, we show in Fig. 5 the same distributions for two of the potentials by comparing the linear radial scale (upper panel) with the more extended log scale (lower panel);

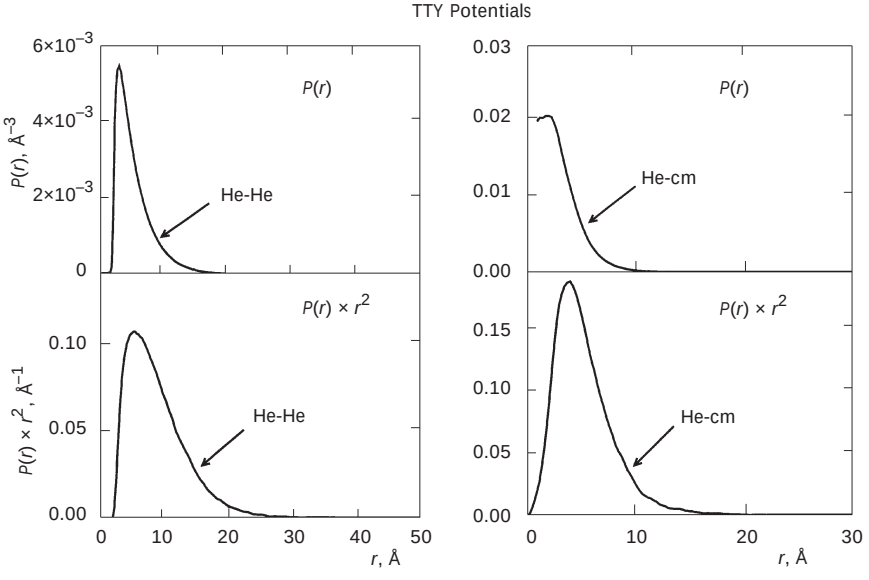

FIG. 4

Computed radial distributions from the present DMC calculations using the TTY 2B potential of ref.[33] Right panel: the upper part reports the ^{4}He distances from the center-of-mass (in Å^{-3}), while the lower part shows the same quantities in Å^{-1}

(iii) the radial distributions from the center-of-mass (r_{cm}), are shown in the upper-right panels and undergo a very marked drop as the distance increases, levelling off to a nearly constant plateau at the small distances. The numerical accuracy for very small r values becomes doubtful and therefore we have not shown, being artifacts of the numerics, the marked spikes given there by the calculations[8]. On the other hand, the corresponding $P(r_{cm}) \times r_{cm}^2$ distributions in the lower-right panel do not show this pathological behaviour;

(iv) the configurations where at least one ^{4}He atom is very close to the center-of-mass of the system are seen to be quite important and suggest here, as already discussed for the angular distributions, the presence of either isosceles or scalene triangles with one angle much larger than 90° and the third atom nearly mid-way between the other two. This aspect of the configurational shapes turns out to be rather important and will be further discussed below.

One can also reconstruct individual radial distributions by analysing the $P(r) \times r^2$ values and by assigning them to different radial bins. Thus, one can obtain from it the distributions of r_1, r_2, r_3 with the *proviso* that each distance is chosen such that it satisfies the relations $r_1 \leq r_2 \leq r_3$ in order to be

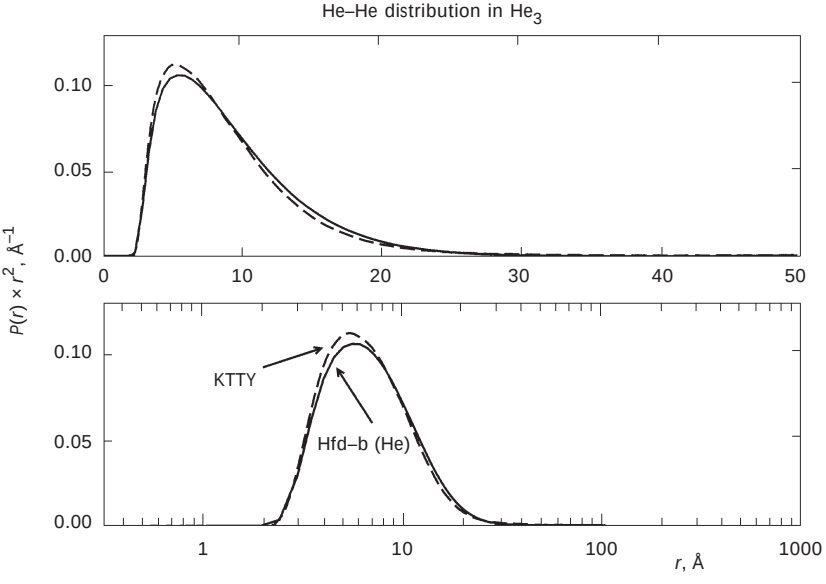

FIG. 5
Computed atom–atom radial distributions for two of the 2B potentials of this study. The lower panel shows the distributions on a radial log scale

selected. The triangular relationship was already satisfied by the DMC calculations of the distributions. To check their numerical quality we run the calculations backward using the radial distributions that we will show below. We therefore reconstructed from them the $P_{tot}(\cos\vartheta)$ *versus* $\cos\vartheta$ distributions discussed before and reproduced the values given by Fig. 3 with a very small numerical error.

The results of the individual radial distributions were again obtained for the four 2B potential functions, but we show in Fig. 6 only the results with the TTY 2B potential. The data are normalized to 1 for the total radial distributions and to 1/3 for each radial distribution, as was also done for the previous angular distributions. The left-hand panel reports the radial data in units of $Å^{-3}$ while the right-hand panel shows them in units of $Å^{-1}$.

The following considerations could be made:

(i) the smallest of the triangular sides shows always the narrowest distribution which peaks below 5 Å, for all potentials;

(ii) both the intermediate and larger distances show broader distributions with tails extending our to more than 50 Å, indicating once more the very floppy and extended nature of the present bound state;

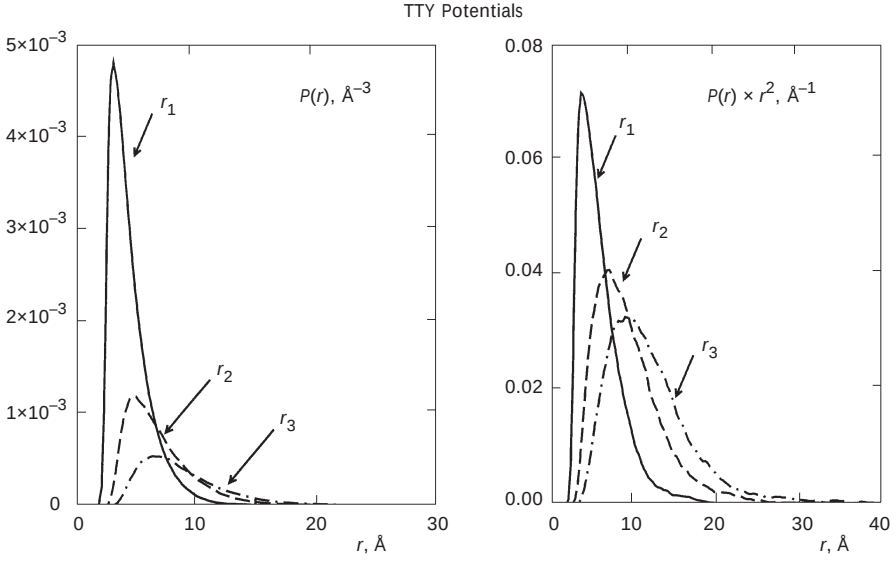

FIG. 6

Computed individual radial distributions for the three sides of the triangular structures. The curves refer to $r_1 < r_2 < r_3$ being selected in the binning. The left panels report probabilities in $Å^{-3}$ while the right panels give them in $Å^{-1}$, each normalized to 1/3. The employed 2B potential is the TTY from ref.[33]

(iii) the peaks of the $P(r)$ distributions are around 5 Å, for r_2 (the intermediate value) and around 7 Å, for the largest side. Such maxima therefore define a scalene triangle as the most likely structure of the triatomic configurations, in contrast with the earlier suggestions of dominant linear[8,39] or equilateral[13] configurations.

However, given the strong floppiness of the present system, it becomes a delicate task to devise methods through which one can still recover a more conventional type of structure. The $P_{tot}(\cos\vartheta)$ distributions, for instance, were analysed in terms of multiple moments of the cosine and found to satisfy the expected values up to the tenth moment, as also found with our earlier DGF calculations[12]. One can also see that the radial and angular distributions of Figs 4–6 follow multimoment distributions which therefore do not necessarily yield maxima which would refer to the same triangle for each radial variable.

We, however, have made a further attempt at analysing the radial distributions on the right-hand panels of Fig. 6 by selecting within them the relative weights of specific triangular structures, chosen according to the five shapes that one can expect to find. They correspond to: equilateral (E), the linear (L), to two different isoscele structures (I_1 and I_2) and to the scalene (S) shape, all of fairly obvious definition.

In order to make a realistic partitioning of such rigid structures which could be extracted from the radial distributions computed with the DMC procedure, we have employed a random number generating routine and separately binned the resulting weights of the triangles defined above.

In order to choose different levels of "rigidity" in the constraining relations employed to define the above triangular structures, we have further included a variable tolerance parameter, Δ, which allows to employ broader acceptance widths of distances values compatible with a given triangular shape. We have selected four Δ values, going from 0 up to 10%. The results of the calculations (which employed about 100,000 random values in the binning search) are reported in Table II for all the 2B potentials. One clearly sees the following:

(i) when the constraint conditions are applied very strictly, *i.e.* the zero tolerance case, one sees that more than 80% of the structures correspond to scalene triangles with only 13% of isosceles structures and no linear configurations;

(ii) when the tolerance level is increased to 1 and 5% we can see that all calculations strongly reduce the presence of S structures with a marked increase of both isosceles and linear configurations. However, the equilateral triangles remain of negligible importance;

TABLE II
Relative percentage of the triangular configurations selected in Fig. 4 as a function of the parameter Δ

Δ	0%	1%	5%	10%
Hfd–B (He)				
E	0.40	0.40	0.70	2.33
I_1	5.65	5.65	5.82	8.53
I_2	11.30	11.30	17.94	30.01
L	0.00	0.11	9.34	19.22
S	82.63	82.51	66.18	39.89
KTTY				
E	0.32	0.32	1.49	4.05
I_1	3.74	3.76	6.15	8.64
I_2	9.15	9.15	20.35	32.31
L	0.00	0.79	6.92	14.09
S	86.76	85.98	65.07	40.89
LM2M2				
E	0.34	0.34	1.54	4.19
I_1	3.5924	3.5766	6.0826	8.44
I_2	9.54	9.54	21.27	33.56
L	0.00	0.84	6.67	13.59
S	86.50	85.67	64.42	40.18
TTY				
E	0.34	0.34	1.49	3.96
I_1	3.59	3.57	6.01	8.50
I_2	8.94	8.94	20.26	32.40
L	0.00	0.88	6.89	14.00
S	87.11	86.24	65.32	41.130

(iii) to further raise the tolerance level up to 10%, as was estimated to be in the earlier DGF calculations[6,12], produces rather dramatic changes in the distributions since S structures are now scaled down to about 40% only. On the other hand, the $I_1 + I_2$ weights increase to around 40% as well, with further appearance of nearly 20% of linear structures. The E configurations, however, remain always of little importance. This unusual presence of linear structures is typical of the $^4He_3$ system and was not found in similar calculations on mixed trimers of the XHe_2 type recently analysed by us[14].

The above analysis of the DMC partial radial distributions shows the importance of the initial tolerance choice made when talking about configurational analysis: the marked dominance of scalene triangular structures is clearly seen from all 2B potential results, while the latter could easily be considered either isosceles or linear if we lowered the tolerance level, *i.e.* weakened the "rigidity" parameter in the chosen structures. Clearly such results are very different from the more conventional picture of a unique "molecular structure" as given by an ensemble of conventional atomic partners which interact with each other in any stable molecule.

Trimer Energetics for the Ground State

Many different theoretical methods and interaction potentials have been used in the last years to obtain the total binding energies of $^4He_3$ trimer. In Table III we have gathered our DMC calculations together with those given by various other approaches. In all calculations, the triatomic potential energy surface has been built as a simple sum of 2B interactions.

An inspection of the Table III shows fairly good agreement among the different theoretical methods (DMC, FE, VM and HC, the acronyms of which are explained there), when they employ the same 2B potential with the exception of the calculations with the KTTY 2B function where we get the largest binding energy value as a result of the potential differences mentioned above.

One can therefore see that essentially all the employed theoretical approaches are able, within the same choice of a given 2B potential, to yield binding energy values for the ground state of this system that agree well with each other. Furthermore, the foregoing discussion has shown that the energy values associated with the lowest bound state of this very special system are much more sensitive to the 2B potential choice than the spatial properties which could be extracted from the corresponding wavefunctions and which are essentially given in a similar manner by all four potential functions examined here.

CONCLUSIONS

In this study we have carried out extensive DMC calculations to evaluate the ground state quantum wavefunction of $^4He_3$ *via* four different PES constructed as sums of 2B potentials. We have also obtained the binding energy values and have compared the present findings with earlier calculations. The differences between binding energies are very dependent on the choice of the 2B potential, while the different methods with the same 2B interaction yield essentially the same energy values.

Our DMC results with three of the 2B potentials are in agreement with earlier studies while, on the other hand, the KTTY proposal of ref.[35] turns out to have too strong a well and to yield a binding energy lower than the other potentials.

Making use of these wavefunctions we have then analysed the angular and radial distributions produced by the calculations. Such data indicate that both the equilateral and the linear structures are not the dominant ones, in contrast with earlier suggestions[8,39,40] while rather "flat" scalene triangles are shown to have the largest probabilities within the configuration distributions.

TABLE III
Computed ground state binding energies (E_b) of $^4He_3$ using the 2B interaction potentials discussed in the present work (all values in cm^{-1})

Computation	Hfd–b (He)[a]	LM2M2[b]	TTY[c]	KTTY[d]
DMC, present	–0.0919(7)[e]	–0.0869(1)[f]	–0.0876(5)[g]	–0.1464(4)[h]
DMC, from ref.[8]	–0.0910(5)	–	–0.0872(4)	–
DMC, from ref.[19]	–0.0924(4)	–	–	–
DMC, from ref.[36]	–	–	–0.08784(7)	–
FE[i], from ref.[10]	–0.0920(9)	–0.0875(0)	–0.0874(3)	–
FE[i], from ref.[29]	–0.0920(4)	–0.0878(5)	–0.0878(5)	–
FE[i], from ref.[25]	–	–0.0870(2)	–	–
VM[j], from ref.[22]	–0.0829(2)	–	–	–
HC[k], from ref.[5]	–	–0.07367(7)	–	–
HC[k], from ref.[13]	–	–0.0870	–	–

[a] From ref.[30]; [b] from ref.[32]; [c] from ref.[33]; [d] from ref.[34]; [e] error: ±0.000389, correlation length: 1.062; [f] error: ±0.000369, correlation length: 1.050; [g] error: ±0.000362, correlation length: 1.073; [h] error: ±0.000546, correlation length: 1.077; [i] Faddeev equations; [j] variational methods; [k] hyperspherical coordinates.

Our results of Table II indicate that the system could be described as being chiefly a scalene triangle and that the use of less rigid triangular shapes shifts a substantial amount of such structures into isosceles and quasi-linear contributions but not into equilateral triangles.

The present study underscores the very special nature of the $^4He_3$ system and the delicate balance existing between the weak interactions among its identical components and the highly quantum nature of its bound state. This feature is indeed responsible for the difficulty in defining its spatial shape *via* a conventional structural language.

The financial support of the Italian National Resarch Council (CNR), of the Italian Ministery for University and Research (MURST) and the Max-Planck Gesellschaft, through the 1995 Research Prize to F. A. Gianturco, are gratefully acknowledged. The Intensive Action Programme between Spain and Italy (2000–2001) is also acknowledged for its support, as well as the DGCYT (Spain) under contract PB95-007 and The European TMR network under contract MPRN-CT-19999-0005. We also thank Dr. F. Paesani for his computational help in the early stages of the present work.

REFERENCES

1. Grebenev S., Toennies J. P., Vilesov A. F.: *Science* **1998**, *279*, 2083.
2. Lehman K. K., Scoles G.: *Science* **1998**, *279*, 2065.
3. Schollkopf W., Toennies J. P.: *Science* **1994**, *266*, 1345.
4. Luo F., McBane G. C., Kim G., Giese C. F., Gentry W. R.: *J. Chem. Phys.* **1994**, *100*, 4023.
5. Esry B. D., Lin C. D., Green C. H.: *Phys. Rev. A: At., Mol., Opt. Phys.* **1996**, *54*, 394.
6. Gonzalez-Lezana T., Rubajo-Soneira J., Miret-Artés S., Gianturco F. A., Delgado-Barrio G., Villarreal P.: *Phys. Rev. Lett.* **1999**, *82*, 1648.
7. Janzen A. R., Aziz R. A.: *J. Chem. Phys.* **1997**, *107*, 914.
8. Lewerenz M.: *J. Chem. Phys.* **1997**, *106*, 4596.
9. Grisenti R. E., Schöllkopf W., Toennies J. P., Hegerfeldt G. C., Köler T., Soll M.: *Phys. Rev. Lett.* **2000**, *85*, 2284.
10. Motovilov A. K., Sandhas W., Sofianos S. A., Kolganova E. A.: *Eur. Phys. J. D* **2001**, *13*, 33.
11. Efimov V.: *Nucl. Phys. A* **1973**, *210*, 157.
12. Gonzalez-Lezana T., Rubajo-Soneira J., Miret-Artés S., Gianturco F. A., Delgado-Barrio G., Villarreal P.: *J. Chem. Phys.* **1999**, *110*, 9000.
13. Blume D., Green C. H., Esry B. D.: *J. Chem. Phys.* **2000**, *113*, 2145.
14. Di Paola C., Gianturco F. A., Paesani F., Delgado-Barrio G., Miret-Artés S., Villarreal P., Baccarelli I., Gonzalez-Lezana T.: *J. Phys. B: At., Mol. Opt. Phys.* **2002**, *35*, 2643.
15. Anderson J.: *J. Chem. Phys.* **1975**, *63*, 1499.
16. Hammond B. L., Lester W. A., Jr., Reynolds P. J.: *Monte Carlo Methods in Ab Initio Quantum Chemistry*. World Scientific, Singapore 1994.
17. Ceperley D. M., Alder B.: *Science* **1986**, *231*, 555.
18. Suhm M. A., Watts R. O.: *Phys. Rev.* **1991**, *204*, 293.
19. Barnett R. N., Whaley K. B.: *J. Chem. Phys.* **1992**, *96*, 2953.

20. Blume D., Lewerenz M., Huisken F., Kaloudis M.: *J. Chem. Phys.* **1996**, *105*, 8666.
21. Reynolds P. J., Ceperley D. M., Alder B., Lester W. A., Jr.: *J. Chem. Phys.* **1982**, *77*, 5593.
22. Rick S. W., Lynch D. L., Doll J. D.: *J. Chem. Phys.* **1991**, *95*, 3506.
23. Pandharipande V. R., Zabolitcky J. G., Pieper S. C., Wiringa R. B., Helmbrecht U.: *Phys. Rev. Lett.* **1983**, *50*, 1676.
24. Guardiola R., Portesi M., Navarro J.: *LANL* – e.print physics/9904037.
25. Nielsen E., Fedorov D. V., Jensen A. S.: *J. Phys. B: At., Mol. Opt. Phys.* **1998**, *31*, 4085.
26. Nakaichi-Malda S., Lim T. K.: *Phys. Rev. A: At., Mol., Opt. Phys.* **1983**, *28*, 692.
27. Cornelius Th., Glöcke W.: *J. Chem. Phys.* **1986**, *85*, 3906.
28. Carbonell J., Gignoux C., Merkuriev S. P.: *Few-Body Systems* **1993**, *15*, 15.
29. Roudnev V., Yakovlev S.: *LANL* – e.print physics/9910030.
30. Aziz R. A., Mc Court F. R. W., Wong C. C. K.: *Mol. Phys.* **1987**, *61*, 1487.
31. Ceperly D. M., Partridge H. J.: *J. Chem. Phys.* **1974**, *61*, 1658.
32. Aziz R. A., Slaman M. J.: *J. Chem. Phys.* **1991**, *94*, 8047.
33. Tang K. T., Toennies J. P., Yiu C. L.: *Phys. Rev. Lett.* **1995**, *74*, 1546.
34. Kleinekathöfer U., Tang K. T., Toennies J. P., Yiu C. L.: *Chem. Phys. Lett.* **1996**, *249*, 257.
35. Kleinekathöfer U., Tang K. T., Toennies J. P., Yiu C. L.: *J. Chem. Phys.* **1997**, *107*, 9502.
36. Kleinekathöfer U., Lewerenz M., Mladenovic M.: *Phys. Rev. Lett.* **1999**, *83*, 4717.
37. Anderson J. B.: *J. Chem. Phys.* **2001**, *115*, 4546.
38. Gdamitz H.: *Mol. Phys.* **2001**, *99*, 923.
39. Casalegno M., Mella M., Morosi G., Bressanini D.: *J. Chem. Phys.* **2000**, *112*, 69.
40. Lee T. G., Esry B. D., Gou B.-C., Lin C. D.: *J. Phys. B: At., Mol. Opt. Phys.* **2001**, *34*, L1.